



Orange-red and white-emitting diodes fabricated by vacuum evaporation deposition of sublimable cationic iridium complexes

Journal:	<i>Journal of Materials Chemistry C</i>
Manuscript ID	TC-ART-02-2016-000738.R2
Article Type:	Paper
Date Submitted by the Author:	12-Apr-2016
Complete List of Authors:	Ma, Dongxin; Tsinghua University, Chemistry Duan, Lian; Tsinghua University, Qiu, Yong; Tsinghua University,



ARTICLE

Orange-red and white-emitting diodes fabricated by vacuum evaporation deposition of sublimable cationic iridium complexes

Dongxin Ma, Lian Duan* and Yong Qiu

Received 00th January 20xx,
Accepted 00th January 20xx

DOI: 10.1039/x0xx00000x

www.rsc.org/

Two novel red-emitting cationic iridium complexes [Ir(ppy)₂(pop)][B(5fph)₄] (**1**) and [Ir(ppy)₂(pop)][BARF₂₄] (**2**) have been developed, here ppy is 2-phenylpyridine, pop is 2-(5-phenyl-1-1,3,4-oxadiazol-2-yl)pyridine, [B(5fph)₄] is terakis(pentafluorophenyl)borate and [BARF₂₄] is terakis[3,5-bis(trifluoromethyl)phenyl]borate, respectively. Photophysical properties of **1** and **2** in both solution and neat film were fully investigated, along with their photochemical, thermal and electrochemical stability. Interestingly, by introducing bulky tetraphenylborate derivatives as negative counter-ions, volatility of **1** and **2** has been extremely improved, enabling fabrication of organic light-emitting diodes (OLEDs) by vacuum evaporation deposition. Doping these two sublimable cationic emitters into the DIC-TRZ (2,4-diphenyl-6-bis(12-phenylindolo[2,3-a]carbazole-11-yl)-1,3,5-triazine) host, we succeeded in the preparation of orange-red-emitting devices with a peak wavelength of 596 nm. **1**-based OLEDs showed a current efficiency of 4.5 cd A⁻¹ and maximum brightness of 19.4 × 10³ cd m⁻², while **2**-based OLEDs furnished a higher efficiency of 5.1 cd A⁻¹. Then we attained white emission by doping **1** or **2** into the TCTA (4,4',4''-tris(carbazol-9-yl)triphenylamine) host at a low concentration. **1**-based white device featured a high colour rendering index (CRI) of 86 and good Commission International de l'Eclairage (CIE) coordinates of (0.33, 0.34), quite close to the equal-energy-white-point (*i. e.*, CIE_{x,y} = 0.33, 0.33), and **2**-based white device showed a rather higher CRI of 89. To our knowledge, this is the first report of white OLEDs fabricated by vacuum evaporation deposition of sublimable cationic iridium complexes, indicating their great potential for full-colour flat-panel display and lighting applications.

Introduction

Since reported by C. W. Tang in 1987, organic light-emitting diodes (OLEDs) have drawn wide attention owing to their technological advantages such as self-emission, fast response and simple device architecture with potential in high-quality flat displays and solid-state lighting.¹ Compared with fluorescent emitters,² OLEDs based on phosphorescent dyes are superior to harvest both the electrogenerated single and triplet excitons thus achieve internal quantum efficiency of nearly 100%.³⁻⁴ Neutral heavy-metal compounds, such as ruthenium,⁵ osmium,^{6,7} iridium⁸⁻¹² and platinum¹³⁻¹⁵ complexes are the most common phosphorescent materials because their strong spin-orbit coupling allows the spin-forbidden triplet excitons to decay radiatively thus improves the overall electroluminescent (EL) efficiency. In recent years, ionic transition metal complexes (iTMCs) with ease of synthesis and wide colour tunability^{16,17} have emerged as a novel class of favourable triplet emitters for OLEDs. Among them, cationic

iridium complexes feature excellent photophysical and electrochemical properties and show efficient luminescence with virtually all colours, thus emerge as by far the most versatile family of iTMCs.¹⁸⁻²³ However, previously demonstrated cationic iridium complexes were seldom evaporable due to the intrinsic ionic nature and low vapour pressure, which severely limited their applications in state-of-the-art OLEDs fabricated by vacuum evaporation deposition.

Moreover, to construct white OLEDs, two or even three emitters are always required in a sophisticated device configuration, which quite complicates fabrication processes thus increases manufacturing costs. Efforts have focused on developing of simple-structured white OLEDs. Forrest and his co-workers first demonstrated the so-called hybrid white OLEDs consisting a blue fluorophore and red phosphorescent dopants²⁴ and Anzenbacher *et al.* then reported a single-red-dopant host-guest system towards high colour rendering index (CRI) of 87.²⁵ However, producing high CRI (> 85) white light with simple device configurations still remains great challenge, and the key prerequisite would be development of red-emitting phosphors.²⁶⁻³⁰

Very recently we reported a facile and feasible molecular design strategy to achieve sublimable cationic iridium complexes by introducing bulky tetraphenylborate derivatives as negative counter-ions.³¹ In this article, we further developed two novel sublimable cationic iridium complexes to

Key Lab of Organic Optoelectronics and Molecular Engineering of Ministry of Education, Department of Chemistry, Tsinghua University, Beijing 100084, P. R. China. *E-mail: duanl@mail.tsinghua.edu.cn; Fax: +86-10-62795137; Tel: +86-10-62788802.

† Electronic Supplementary Information (ESI) available: [Experimental (methods and instrumentation, device fabrication and characterization), Schemes S1 and Figures S1-S8]. See DOI: 10.1039/x0xx00000x

fabricate orange-red-emitting OLEDs by vacuum evaporation deposition thereof. What is more, by optimizing doping concentrations and choosing suitable hosts, we obtained single-dopant white-emitting OLEDs with good colour coordinates of (0.33, 0.34) and an exceptionally high CRI of 89.

Experimental

Synthetic procedures

All the reactants and solvents were purchased from commercial sources and used as received unless otherwise stated.

Synthesis and characterization of 1. The pop ligand was synthesized from its hydrazide precursor according to a previous literature.³² The dichloro-bridged diiridium complex $[\text{Ir}(\text{ppy})_2\text{Cl}]_2$ (0.576 g, 0.54 mmol) and pop ligand (0.243 g, 1.09 mmol) were dissolved in 60 mL methanol/ CH_2Cl_2 ($v/v = 1:1$) mixed-solution. The mixture was then refluxed at 50 °C for 6 h under an argon atmosphere to form a clear red solution. After cooling to room temperature, $\text{Na}[\text{B}(\text{5fph})_4]$ (0.870 g, 1.23 mmol) was slowly added into the reaction mixture under stirring. The reaction liquid was filtered, evaporated, then dried under vacuum at 70 °C overnight. The crude product was purified by column chromatography on silica gel (200-300 mesh) with CH_2Cl_2 as the eluent, yielding a red powder (1.024 g, 0.77 mmol). Yield: 74 %. Characterization in the pristine state: $^1\text{H-NMR}$ (600 MHz, $\text{DMSO-}d_6$): δ 8.73 (d, $J = 7.7$ Hz, 1H), 8.43 (td, $J = 7.7$ Hz, 1.6 Hz, 1H), 8.32 (d, $J = 5.2$ Hz, 1H), 8.27 (d, $J = 8.0$ Hz, 2H), 8.18 (d, $J = 7.3$ Hz, 2H), 7.99 (t, $J = 7.8$ Hz, 2H), 7.93 (d, $J = 7.6$ Hz, 1H), 7.91-7.86 (m, 3H), 7.76 (t, $J = 7.5$ Hz, 1H), 7.69 (dd, $J = 15.8$ Hz, 7.5 Hz, 3H), 7.23 (ddd, $J = 6.0$ Hz, 4.5 Hz, 2.2 Hz, 2H), 7.06 (dd, $J = 9.7$ Hz, 5.3 Hz, 1H), 6.99 (t, $J = 7.5$ Hz, 1H), 6.94 (t, $J = 7.5$ Hz, 1H), 6.86 (t, $J = 7.4$ Hz, 1H), 6.17 (dd, $J = 12.0$ Hz, 7.6 Hz, 2H). $^{19}\text{F-NMR}$ (600 MHz, $\text{DMSO-}d_6$): δ -133.30 (s, 8F), -161.68 (s, 4F), -166.65 (s, 8F). MS (ESI) [m/z]: $[\text{M-B}(\text{5fph})_4]^+$ calcd for $\text{C}_{35}\text{H}_{25}\text{IrN}_5\text{O}$, 724.17; found, 724.17; $[\text{M-Ir}(\text{ppy})_2(\text{pop})]^+$ calcd for $\text{C}_{24}\text{BF}_{20}$, 678.97; found, 678.98. Characterization after sublimation: $^1\text{H-NMR}$ (600 MHz, $\text{DMSO-}d_6$): δ 8.69 (d, $J = 7.9$ Hz, 1H), 8.42-8.37 (m, 1H), 8.27 (d, $J = 6.0$ Hz, 1H), 8.23 (d, $J = 8.2$ Hz, 2H), 8.13 (d, $J = 7.2$ Hz, 2H), 7.97-7.92 (m, 2H), 7.89 (d, $J = 7.9$ Hz, 1H), 7.85-7.82 (m, 3H), 7.72 (t, $J = 7.2$ Hz, 1H), 7.66-7.61 (m, 3H), 7.20-7.17 (m, 2H), 7.03-7.01 (m, 1H), 6.97-6.93 (m, 1H), 6.90 (td, $J = 7.5$, 1.2 Hz, 1H), 6.82 (td, $J = 7.5$, 1.2 Hz, 1H), 6.11 (dd, $J = 12.6$, 7.2 Hz, 2H); $^{19}\text{F-NMR}$ (600 MHz, $\text{DMSO-}d_6$): δ -132.34 (s, 8F), -161.17 (s, 4F), -165 (s, 8F). MS (ESI) [m/z]: $[\text{M-B}(\text{5fph})_4]^+$ calcd for $\text{C}_{35}\text{H}_{25}\text{IrN}_5\text{O}$, 724.17; found, 724.17; $[\text{M-Ir}(\text{ppy})_2(\text{pop})]^+$ calcd for $\text{C}_{24}\text{BF}_{20}$, 678.97; found, 678.97. Detailed NMR spectra are shown in **Figures S5-6** in the **Electronic Supplementary Information**.

Synthesis and characterization of 2. The dichloro-bridged diiridium complex $[\text{Ir}(\text{ppy})_2\text{Cl}]_2$ (1.775 g, 1.66 mmol) and pop ligand (0.740 g, 3.32 mmol) were dissolved in 60 mL methanol/ CH_2Cl_2 ($v/v = 1:1$) mixed-solution. The mixture was then refluxed at 50 °C for 6 h under an argon atmosphere to form a clear red solution. After cooling to room temperature, $\text{Na}[\text{BArF}_{24}]$ (3.224 g, 3.64 mmol) was slowly added into the reaction mixture under stirring. The reaction liquid was filtered, evaporated, then dried under vacuum at 70 °C overnight. The crude product was purified by column

chromatography on silica gel (200-300 mesh) with CH_2Cl_2 as the eluent, yielding a red powder (4.551 g, 2.87 mmol). Yield: 87 %. Characterization in the pristine state: $^1\text{H-NMR}$ (600 MHz, $\text{DMSO-}d_6$): δ 8.68 (d, $J = 7.7$ Hz, 1H), 8.38 (td, $J = 7.8$ Hz, 2.1 Hz, 1H), 8.26 (d, $J = 5.5$ Hz, 1H), 8.22 (d, $J = 8.5$ Hz, 2H), 8.14-8.10 (m, 2H), 7.94 (t, $J = 7.8$ Hz, 2H), 7.88 (d, $J = 8.7$ Hz, 1H), 7.86-7.81 (m, 3H), 7.72 (d, $J = 7.4$ Hz, 1H), 7.69 (s, 4H), 7.63 (dd, $J = 13.5$ Hz, 6.1 Hz, 3H), 7.60 (s, 8H), 7.18 (dt, $J = 6.0$ Hz, 4.7 Hz, 2H), 7.01 (t, $J = 7.6$ Hz, 1H), 6.94 (t, $J = 7.6$ Hz, 1H), 6.89 (dd, $J = 8.1$ Hz, 7.1 Hz, 1H), 6.81 (t, $J = 7.5$ Hz, 1H), 6.11 (dd, $J = 11.9$ Hz, 7.5 Hz, 2H). $^{19}\text{F-NMR}$ (600 MHz, $\text{DMSO-}d_6$): δ -61.60 (s, 24F). MS (ESI) [m/z]: $[\text{M-BArF}_{24}]^+$ calcd for $\text{C}_{35}\text{H}_{25}\text{IrN}_5\text{O}$, 724.17; found, 724.16; $[\text{M-Ir}(\text{ppy})_2(\text{pop})]^+$ calcd for $\text{C}_{32}\text{H}_{12}\text{BF}_{24}$, 863.06; found, 863.06. Characterization after sublimation: $^1\text{H-NMR}$ (600 MHz, $\text{DMSO-}d_6$): δ 8.69 (d, $J = 7.8$ Hz, 1H), 8.42-8.36 (m, 1H), 8.28 (d, $J = 5.8$ Hz, 1H), 8.23 (d, $J = 8.3$ Hz, 2H), 8.15-8.12 (m, 2H), 7.95 (t, $J = 7.2$ Hz, 2H), 7.89 (d, $J = 7.2$ Hz, 1H), 7.85-7.83 (m, 3H), 7.72 (d, $J = 7.5$ Hz, 1H), 7.70 (s, 4H), 7.66-7.62 (m, 3H), 7.61 (s, 8H), 7.22-7.16 (m, 2H), 7.04-6.99 (m, 1H), 6.97-6.92 (m, 1H), 6.90 (td, $J = 7.5$, 1.1 Hz, 1H), 6.82 (td, $J = 7.5$, 1.1 Hz, 1H), 6.11 (dd, $J = 12.3$, 7.8 Hz, 2H); $^{19}\text{F-NMR}$ (600 MHz, $\text{DMSO-}d_6$): δ -61.63 (s, 24F). MS (ESI) [m/z]: $[\text{M-BArF}_{24}]^+$ calcd for $\text{C}_{35}\text{H}_{25}\text{IrN}_5\text{O}$, 724.17; found, 724.17; $[\text{M-Ir}(\text{ppy})_2(\text{pop})]^+$ calcd for $\text{C}_{32}\text{H}_{12}\text{BF}_{24}$, 863.06; found, 863.05. Detailed NMR spectra are shown in **Figures S7-8** in the **Electronic Supplementary Information**. Single crystal of **2** was grown from acetone/ methanol mixed-solution and characterized by X-ray crystallography. Space group of P_{21} with $a = 16.505(3)$ Å, $b = 16.849(3)$ Å, $c = 23.262(5)$ Å, $\alpha = 90.00^\circ$, $\beta = 95.08(3)^\circ$, $\gamma = 90.00^\circ$, $V = 6444(2)$ Å³, $Z = 2$, $d_{\text{calcd}} = 1.641$ g cm⁻³, $R_1 = 0.0629$, $\omega R_2 = 0.1268$ for 41866 observed reflections [$I \geq 2\sigma(I)$]. More crystallographic data can be found in CCDC 1046399, which can be obtained free from the Cambridge Crystallographic Data Centre from www.ccdc.cam.ac.uk/conts/retrieving.html.

Results and discussion

Synthesis and structural characterization

Initially we developed two novel sublimable cationic iridium complexes with the same coordinated iridium(III) cation but different bulky counter-ions, $[\text{Ir}(\text{ppy})_2(\text{pop})][\text{B}(\text{5fph})_4]$ (**1**) and $[\text{Ir}(\text{ppy})_2(\text{pop})][\text{BArF}_{24}]$ (**2**), respectively, as shown in **Figure 1a**. These two complexes were synthesized according to the established procedures for cationic iridium complexes, as described in **Scheme S1** in **Electronic Supplementary Information**. In the first step, we utilized IrCl_3 hydrate as the metal source reacting with a 50 % excess of ppy ligand to yield the intermediate dichloro-bridged diiridium complex, which then reacted with pop ligand to afford the cationic iridium complex. Finally, chloridion (Cl^-) was replaced by $[\text{B}(\text{5fph})_4]^-$ or $[\text{BArF}_{24}]^-$ via facile counter-ion exchange reactions to yield **1** or **2**, respectively. Both the two complexes were fully characterized by $^1\text{H-NMR}$, $^{19}\text{F-NMR}$ and ESI mass spectrometry (see **Experimental**).

To further confirm the structural feature, we obtained single crystal of **2** from acetone/ methanol mixed-solution and characterized it by X-ray crystallography. In agreement with the previously reported cationic iridium complexes,^{33,34} the

coordinated iridium(III) cation $[\text{Ir}(\text{ppy})_2(\text{pop})]^+$ shows a distorted octahedral geometry around the iridium center with two cyclometalated ligands (ppy) and one ancillary ligand (pop) adopting *C*, *C-cis*, *N*, *N-trans* configurations, while the negative counter-ion $[\text{BArF}_{24}]^-$ exhibits a regular tetrahedron geometry around the boron atom (see **Figure 1b**). It is notable that distance between iridium and boron of **2** reaches 8.33 Å, suggesting a large ionic radii and weak electrostatic interaction. Quantum chemical calculation results show that volume of $[\text{B}(\text{5fph})_4]^-$ and $[\text{BArF}_{24}]^-$ is quite large, 320.78 and 425.02 cm³ mol⁻¹, respectively.

<Figure 1>

Photophysical, thermal and electrochemical properties

Ultraviolet-visible absorption spectra of **1** and **2** in degassed acetonitrile solution are presented in **Figure 2a**. In ultraviolet (UV) region, the intense absorption bands between 200 and 330 nm are ascribed to spin-allowed $^1\pi\text{-}\pi^*$ transitions from the cyclometalated ligands. The very weak absorption bands from 350 extending to 400 nm correspond to excitations to $^1\text{MLCT}$ (metal-to-ligand charge transfer), $^1\text{LLCT}$ (ligand-to-ligand charge transfer), $^3\text{MLCT}$, $^3\text{LLCT}$ and LC (ligand-centered) $^1\pi\text{-}\pi^*$ transitions. Seen from **Figure 2b**, under excitation **1** and **2** show red emission peaked at ca. 630 nm in acetonitrile solution. The broad and featureless PL spectra indicate that their emissive excited states have predominantly $^3\text{LLCT}$ or $^3\text{MLCT}$ rather than ^3LC $\pi\text{-}\pi^*$ characters.^{35,36} Further experiments suggest the inferior photochemical stability of **1** and **2** in solution (see **Figure S1**), probably due to degradation of both the pop moiety and organic counter-ions,³⁷ while that in solid states seems much better, where UV irradiation only affects the intensity but not the site of phosphorescence peaks (see **Figure S2**).

Then we compared PL spectra of **1** and **2** in neat film, fabricated by spin coating and vacuum evaporation deposition, respectively. As shown in **Figure 2b** and **Table 1**, PL spectra of **1** and **2** in the spin-coated film are peaked at 599 and 597 nm, respectively. And in the evaporated film, **1** and **2** show quite similar emission with a major peak at 600 and 598 nm, respectively, indicating their desirable volatility without observable decomposition. It is worth mentioning that PL spectra of **1** and **2** in neat film are obviously blue-shifted, which might be explained that their bulky counter-ions show quite a weak electric field, less able to stabilize the polar excited states, leading to the pronounced blue shift in solid states. Note that photoluminescent quantum yields (PLQYs) of **1** and **2** in neat film are rather high over 20 %, owing to the decreased intermolecular interactions and reduced concentration quenching by the large-sized counter-ions, as we previously reported.³⁸ Next we dissolved the evaporated film in deuterated dimethyl sulfoxide (DMSO-*d*₆) then characterized $^1\text{H-NMR}$, $^{19}\text{F-NMR}$ spectra and ESI mass spectrometry. The obtained results are quite similar to characterization of **1** and **2** in the pristine state (see **Experimental**), which further demonstrate their good sublimability.

<Figure 2>

Moreover, differential scanning calorimetry (DSC) and thermogravimetric analysis (TGA) performed under a dry nitrogen gas flow at a heating rate of 10 °C/min indicate that **1** and **2** are thermally stable with 5 % weight reduction temperatures of 356 and 293 °C, respectively (see **Figure S3**), enabling their applications in vapour-processed devices. And vacuum mass spectra also proved existence of the coordinated iridium(III) cation $[\text{Ir}(\text{ppy})_2(\text{pop})]^+$ (peaked at 724.2) during vacuum evaporation.

In addition, electrochemical properties of **1** and **2** are also collated in **Table 1**. As described in **Figure S4**, their cyclic voltammogram in degassed N,N-dimethyl formamide (DMF) solution is quite similar, with a reduction potential of ca. -1.6 V and an oxidation potential of ca. 0.9 V, respectively.

<Table 1>

Fabrication and evaluation of OLEDs

To investigate electroluminescent (EL) behaviours of **1** and **2** in devices, first we fabricated OLEDs by vacuum evaporation deposition thereof, with a following structure of ITO/ NPB (40 nm)/ DIC-TRZ: *x* mol. % **1** or **2** (20 nm)/ TPBi (30 nm)/ Mg: Ag (150 nm)/ Ag (50 nm). Here NPB is N, N'-bis(naphthalene-1-yl)-N,N'-bis(phenyl)-benzidine used for hole injection and TPBi (1,3,5-tris(1-phenyl-1*H*-benzo[d]imidazole-2-yl)benzene) was inserted for hole-blocking. To prevent the energy transfer of triplet excitons from the emitters back to the host material, we elected DIC-TRZ (2,4-diphenyl-6-bis(12-phenylindolo[2,3-*a*]carbazole-11-yl)-1,3,5-triazine)⁴⁰ with a triplet energy of 3.0 eV as the bipolar host. Molecular structures and energy level diagram of the used materials in devices are described in **Figure 3**. Doping concentrations of **1** and **2** are varied for optimization, and the tabulated device performance is depicted in **Table 2**.

<Figure 3>

Current density (*J*) and luminance (*L*) versus working voltage (*V*) characteristics of **1**-based OLEDs are presented in **Figure 4**. Note that the *J*-*V* curve shifts towards the low voltages, ascribed to the electron trap caused by ionic materials.¹⁸ **1**-based OLEDs show orange-red emission peaked at 596 nm with CIE coordinates varying a little from (0.52, 0.45) to (0.53, 0.46). At the doping ratio of 6 mol. %, we attained a maximum current efficiency (*CE*) of 4.5 cd A⁻¹ and high brightness of 19.4×10³ cd m⁻². As shown in **Figure 5**, **2**-based OLEDs also emit orange-red with rather similar EL spectra, independent of counter-ions, achieving a higher *CE* of 5.1 cd A⁻¹.

<Figure 4>

<Figure 5>

<Table 2>

Next we doped **1** and **2** into the 4,4',4''-tris(carbazol-9-yl)triphenylamine (TCTA) matrix and fabricated OLEDs with a device configuration changed a little to ITO/ NPB (40 nm)/ TCTA: *y* mol. % **1** or **2** (20 nm)/ TPBi (30 nm)/ Mg: Ag (150 nm)/ Ag (50 nm) (see **Figure 3**). Here TCTA was used not only as a

host material with an optical band gap of 3.4 eV, but also a hole-transporter due to its conjugated structure.⁴¹ As depicted in **Figure 6**, the current density gradually decreases with the doping ratio of **1** increasing from 2 to 10 mol. %, and the associated OLEDs show orange to red emission with the peak wavelength varying from 578 to 608 nm. A maximum CE of 3.4 cd A⁻¹ and brightness of 4.4×10³ cd m⁻² was obtained, a little lower than the corresponding OLEDs with DIC-TRZ host. Analogously, we attained **2**-based red-emitting OLEDs with a maximum CE of 2.8 cd A⁻¹ and brightness of 4.6×10³ cd m⁻² (see **Figure 7**).

Interestingly, when doping **1** into TCTA at a low concentration of 2 mol. %, we obtained white-emitting OLED with a maximum CE of 1.8 cd A⁻¹ and a high CRI of 86. The colour coordinates are (0.33, 0.34), quite close to the equal-energy-white-point (*i. e.*, CIE_{x,y} = 0.33, 0.33). Seen from **Table 3**, EL spectra show a dual emission peaked at 566 nm with a shoulder at 430 nm, and the latter was probably attributed to the TCTA host. With 1 mol. % **2** doped into TCTA, we also achieved white emission with CIE coordinates of (0.32, 0.27) and a rather higher CRI of 89. However, since the white emission arises from an incomplete energy transfer process from the TCTA host and the dopants (**1** or **2**), the obtained device performance is dramatically decreased, particularly in terms of current efficiency.

<Figure 6>

<Figure 7>

<Table 3>

Conclusions

In summary, we designed, synthesized and investigated two novel sublimable red-emitting cationic iridium complexes (**1** and **2**). Through optimizing doping concentrations and wisely choosing suitable host materials, we succeeded in the preparation of orange-red-emitting OLEDs by vacuum evaporation deposition, achieving a maximum CE of 5.1 cd A⁻¹ and high brightness of 19.4×10³ cd m⁻², respectively. Doping **1** and **2** into TCTA host with a wide band gap, we obtained white emission with high CRI values of 86 and 89, respectively. To the best of our knowledge, this is the first report of vacuum-evaporated iTMCs-based white OLEDs. Our study indicates that sublimable cationic iridium complexes are promising phosphorescent materials with immense potential in full-colour display and solid-state lighting.

Acknowledgements

We would like to thank the National Natural Science Fund for Distinguished Young Scholars of China (Grant No. 51525304), the National Key Basic Research and Development Program of China (Grant No. 2015CB655002) for financial support. D. Ma is also grateful for the support of Tsinghua Fudaoyuan Research Fund.

Notes and references

‡ Electronic Supplementary Information (ESI) available: [Experimental (methods and instrumentation, device fabrication and characterization), Scheme S1 and Figures S1-S8]. See DOI: 10.1039/b000000x/

- C. W. Tang and S. A. Vanslyke, *Appl. Phys. Lett.*, 1987, **51**, 913.
- M. Pope, H. P. Kallmann and P. Magnante, *J. Chem. Phys.*, 1963, **38**, 2042.
- L. J. Rothberg and A. J. Lovinger, *J. Mater. Res.*, 1996, **11**, 3174.
- P. -T. Chou and Y. Chi, *Chem. Eur. J.*, 2007, **13**, 380.
- Y. -L. Tung, L. -S. Chen, Y. Chi, P. -T. Chou, Y. -M. Cheng, E. Y. Li, G. -H. Lee, C. -F. Shu, F. -I. Wu and A. J. Carty, *Adv. Funct. Mater.*, 2006, **16**, 1615.
- Y. -M. Cheng, G. -H. Lee, P. -T. Chou, L. -S. Chen, Y. Chi, C. -H. Yang, Y. -H. Song, S. -Y. Chang, P. -I. Shih and C. -F. Shu, *Adv. Funct. Mater.*, 2008, **18**, 183.
- J. -L. Liao, Y. Chi, C. -C. Yeh, H. -C. Kao, C. -H. Chang, M. A. Fox, P. J. Low and G. -H. Lee, *J. Mater. Chem. C.*, 2015, **3**, 4910.
- M. A. Baldo, S. Lamansky, P. E. Burrows, M. E. Thompson and S. R. Forrest, *Appl. Phys. Lett.*, 1999, **75**, 4.
- Y. -J. Su, H. -L. Huang, C. -L. Li, C. -H. Chien, Y. -T. Tao, P. -T. Chou, S. Datta and R. -S. Liu, *Adv. Mater.*, 2003, **15**, 884.
- T. Tsuzuki, N. Shirasawa, T. Suzuki and S. Tokito, *Adv. Mater.*, 2003, **15**, 1455.
- S. -J. Yeh, M. -F. Wu, C. -T. Chen, Y. -H. Song, Y. Chi, M. -H. Ho, S. -F. Hsu and C. H. Chen, *Adv. Mater.*, 2005, **17**, 285.
- C. -F. Chang, Y. -M. Cheng, Y. Chi, Y. -C. Chiu, C. -C. Lin, G. -H. Lee, P. -T. Chou, C. -C. Chen, C. -H. Chang and C. -C. Wu, *Angew. Chem. Int. Ed.*, 2008, **47**, 4542.
- M. A. Baldo, D. F. O'Brien, Y. You, A. Shoustikov, S. Sibley, M. E. Thompson and S. R. Forrest, *Nature*, 1998, **395**, 151.
- Y. Unger, D. Meyer, O. Molt, C. Schildknecht, I. Münster, G. Wagenblast and T. Strassner, *Angew. Chem. Int. Ed.*, 2010, **49**, 10214.
- T. Fleetham, G. Li, L. Wen and J. Li, *Adv. Mater.*, 2014, **26**, 7116.
- R. D. Costa, E. Ortí, H. J. Bolink, F. Monti, G. Accorsi and N. Armaroli, *Angew. Chem. Int. Ed.*, 2012, **51**, 8178.
- E. Holder, B. M. W. Langeveld and U. S. Schubert, *Adv. Mater.*, 2005, **17**, 1109.
- E. A. Plummer, A. Dijken, H. W. Hofstraat, L. D. Cola and K. Brunner, *Adv. Funct. Mater.*, 2005, **15**, 281.
- L. He, L. Duan, J. Qiao, D. Zhang, G. Dong, L. Wang and Y. Qiu, *Org. Electron.*, 2009, **10**, 152.
- L. He, L. Duan, J. Qiao, D. Zhang, L. Wang and Y. Qiu, *Org. Electron.*, 2010, **11**, 1185.
- D. Ma, L. Duan, Y. Wei and Y. Qiu, *Chem. Eur. J.*, 2014, **20**, 15903.
- Y. Wu, H. -Z. Sun, H. -T. Cao, H. -B. Li, G. -G. Shan, Y. -A. Duan, Y. Geng, Z. -M. Su and Y. Liao, *Chem. Commun.*, 2014, **50**, 10986.
- D. Ma, L. Duan and Y. Qiu, *Dalton. Trans.*, 2015, **44**, 8521.
- Y. Sun, N. C. Giebink, H. Kanno, B. Ma, M. E. Thompson and S. R. Forrest, *Nature*, 2006, **440**, 908.
- P. Anzenbacher Jr., V. A. Montes and S. Takizawa, *Appl. Phys. Lett.*, 2008, **93**, 163302.
- T. Peng, Y. Yang, H. Bi, Y. Liu, Z. Hou and Y. Wang, *J. Mater. Chem.*, 2011, **21**, 3551.
- J. Li, R. Wang, R. Yang, W. Zhou and X. Wang, *J. Mater. Chem. C.*, 2013, **1**, 4171.
- B. Liu, M. Xu, L. Wang, J. Zou, H. Tao, Y. Su, D. Gao, H. Ning, L. Lan and J. Peng, *Org. Electron.*, 2014, **15**, 2616.
- L. Y. Guo, X. L. Zhang, H. S. Wang, C. Liu, Z. G. Li, Z. J. Liao, B. X. Mi, X. H. Zhou, C. Zheng, Y. H. Li and Z. Q. Gao, *J. Mater. C.*, 2015, **3**, 5412.

- 30 H. Cao, G. Shan, X. Wen, H. Sun, Z. Su, R. Zhong, W. Xie, P. Li and D. Zhu, *J. Mater. Chem. C*, 2013, **1**, 7371.
- 31 D. Ma, Y. Qiu and L. Duan, *Adv. Funct. Mater.*, 2016, doi: 10.1002/adfm.201505493.
- 32 J. Zhang, L. Zhou, H. A. Al-Attar, K. Shao, L. Wang, D. Zhu, Z. Su, M. R. Bryce and A. P. Monkman, *Adv. Funct. Mater.*, 2013, **23**, 4667.
- 33 J. D. Slinker, A. A. Gorodetsky, M. S. Lowry, J. Wang, S. Parker, R. Rohl, S. Bernhard and G. G. Malliaras, *J. Am. Chem. Soc.*, 2004, **126**, 2763.
- 34 M. S. Lowry, W. R. Hudson, R. A. Pascal Jr. and S. Bernhard, *J. Am. Chem. Soc.*, 2004, **126**, 14129.
- 35 M. G. Colombo and H. U. Güdel, *Inorg. Chem.*, 1993, **32**, 3081.
- 36 M. G. Colombo, A. Hauser and H. U. Güdel, *Inorg. Chem.*, 1993, **32**, 3088.
- 37 M. Mauro, M. Panigati, D. Donghi, P. Mercandelli, P. Mussini, A. Sironi and G. D'Alfonso, *Inorg. Chem.*, 2008, **47**, 11154.
- 38 D. Ma, L. Duan, Y. Wei, L. He, L. Wang and Y. Qiu, *Chem. Commun.*, 2014, **50**, 530.
- 39 L. J. Charbonnière, S. Faulkner, C. Platas-Iglesias, M. Regueiro-Figueroa, A. Nonat, T. Rodríguez-Blas, A. Blas, W. S. Perry and M. Tropicano, *Dalton. Trans.*, 2013, **42**, 3667.
- 40 D. Zhang, L. Duan, C. Li, Y. Li, D. Zhang and Y. Qiu, *Adv. Mater.*, 2014, **26**, 5050.
- 41 D. Qin and Y. Tao, *Appl. Phys. Lett.*, 2005, **86**, 113507.

Figure 1. (a) Chemical structures of **1** and **2**, (b) single crystal of **2**. Here ppy is 2-phenylpyridine, pop is 2-(5-phenyl-1,3,4-oxadiazol-2-yl)pyridine, $[B(5fph)_4]^-$ is tetrakis(pentafluorophenyl)borate and $[BArF_{24}]^-$ is tetrakis[3,5-bis(trifluoromethyl)phenyl]borate. In the single crystal, thermal ellipsoids are drawn at 30 % probability. The solvent molecules and hydrogen atoms are omitted for clarity. The unlabeled atoms are carbon atoms.

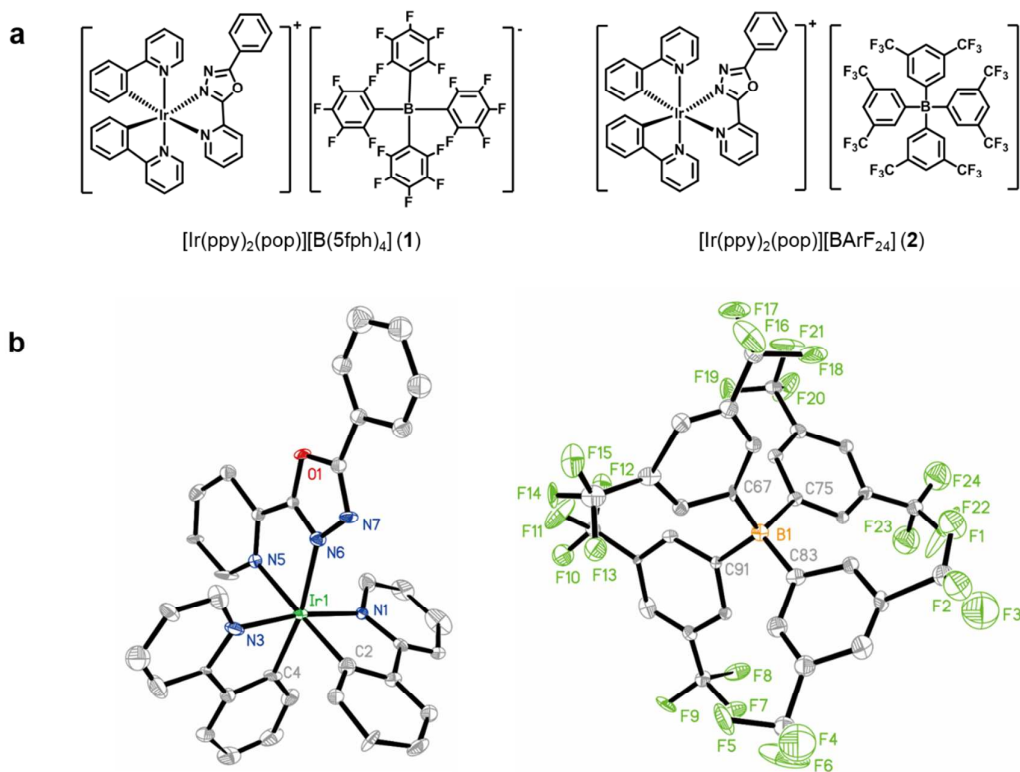


Figure 2. (a) Absorption in acetonitrile solution (10^{-5} M) and (b) normalized photoluminescence spectra of **1** and **2** in acetonitrile solution (red square), spin-coated (olive circle) and vacuum-evaporated (blue triangle) neat film, respectively.

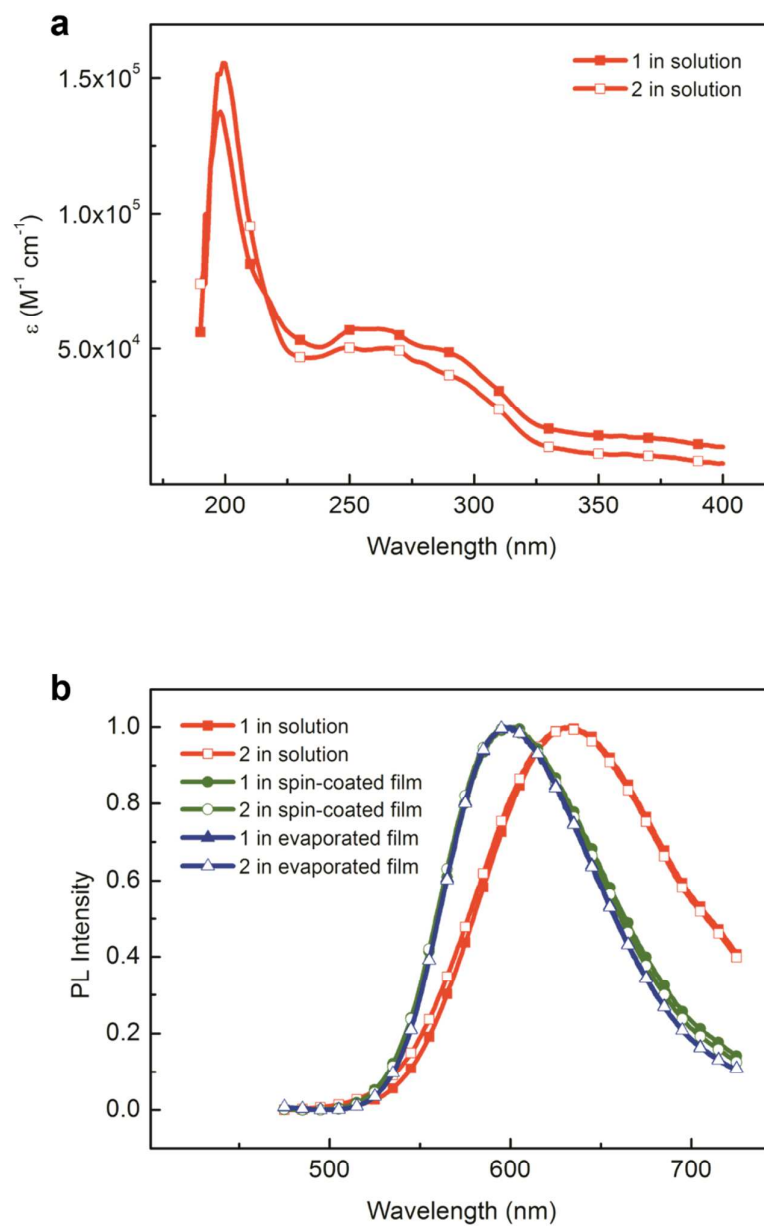


Figure 3. (a) Molecular structures and (b) energy level diagram of materials used in OLEDs. Here NPB is N, N'-bis(naphthalene-1-yl)-N,N'-bis(phenyl)-benzidine, DIC-TRZ is 2,4-diphenyl-6-bis(12-phenylindolo)[2,3-a]carbazole-11-yl-1,3,5-triazine, TCTA is 4,4',4''-tris(carbazol-9-yl)triphenylamine, and TPBi is 1,3,5-tris(1-phenyl-1*H*-benzo[d]imidazole-2-yl)benzene.

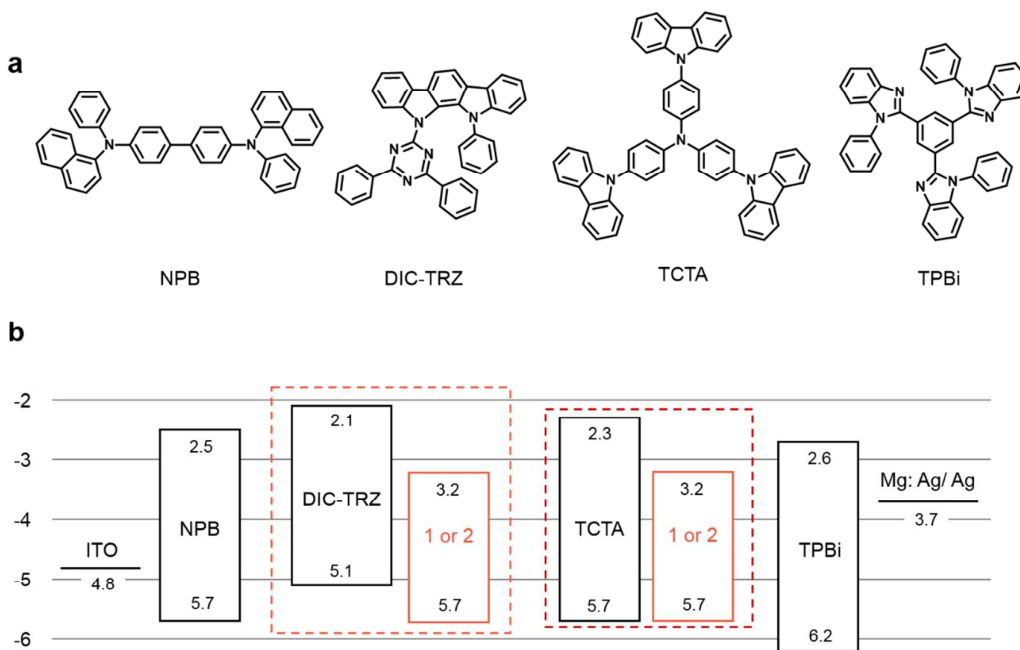


Figure 4. (a) *J-V*, (b) *L-V* characteristics and (c) normalized EL spectra of OLEDs with a structure of ITO/ NPB (40 nm)/ DIC-TRZ: *x* mol. % **1** (20 nm)/ TPBi (30 nm)/ Mg: Ag (150 nm)/ Ag (50 nm), *x* = 4, 6 or 8.

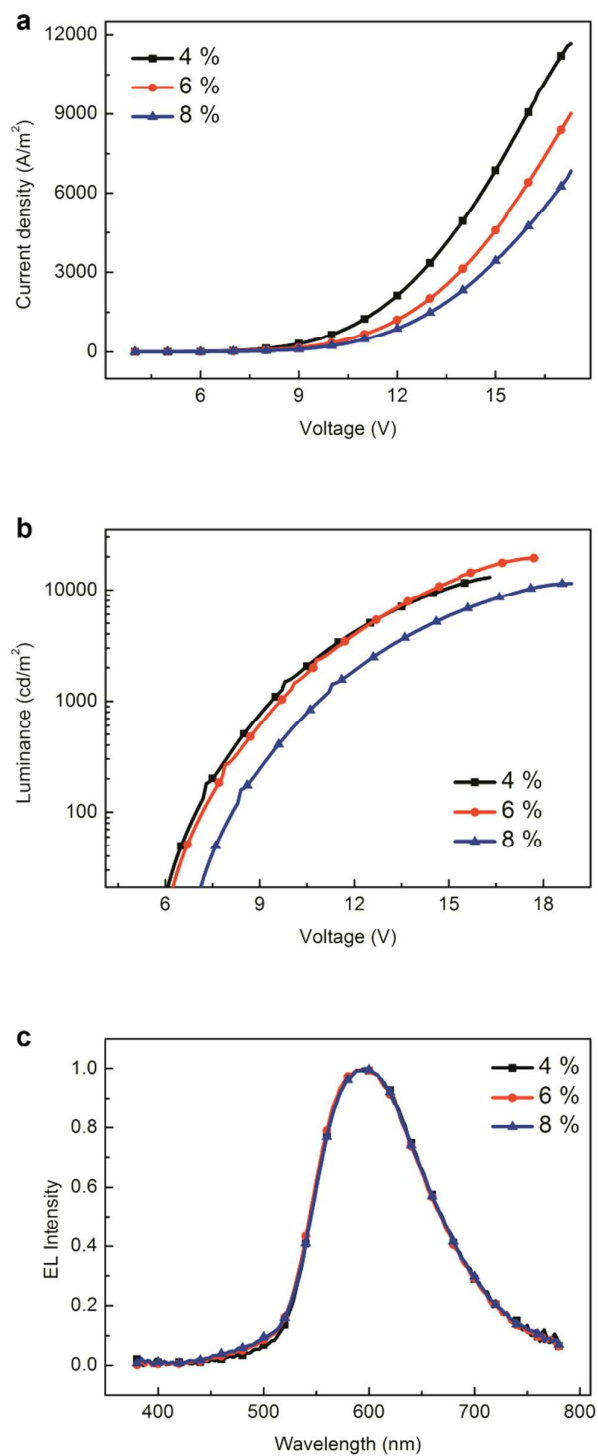


Figure 5. (a) *J-V*, (b) *L-V* characteristics and (c) normalized EL spectra of OLEDs with a structure of ITO/ NPB (40 nm)/ DIC-TRZ: *x* mol. % **2** (20 nm)/ TPBi (30 nm)/ Mg: Ag (150 nm)/ Ag (50 nm), *x* = 4, 6, 8 or 10.

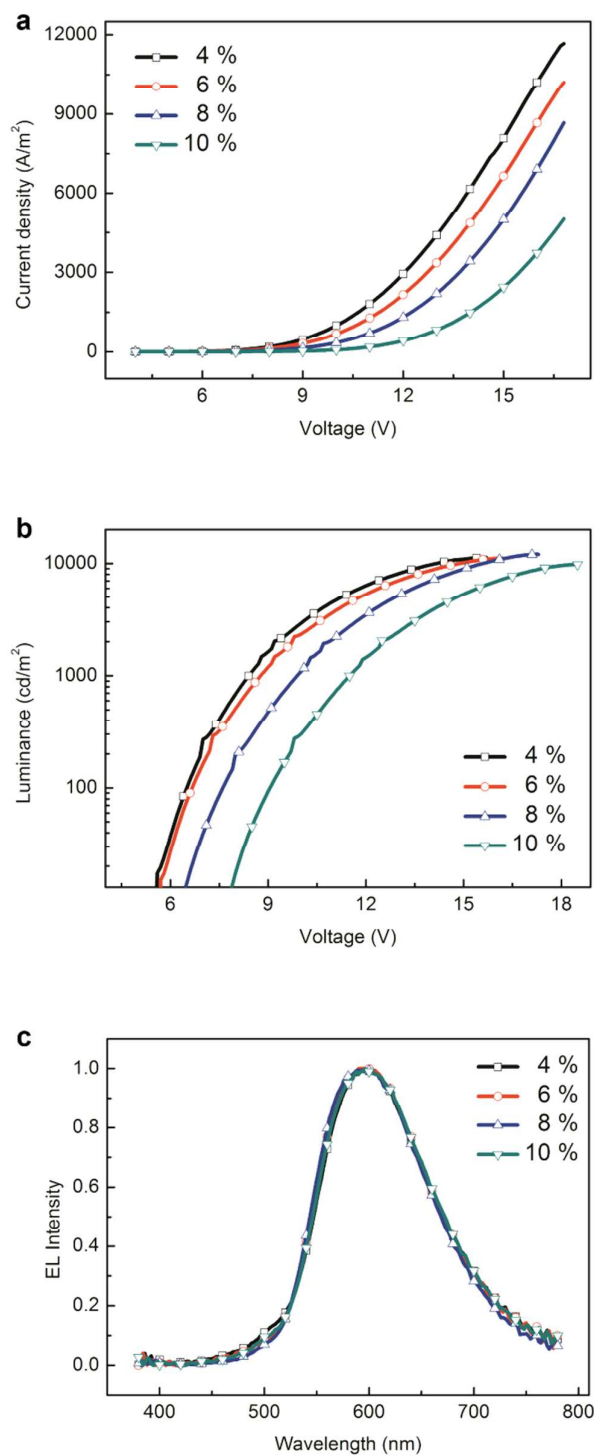


Figure 6. (a) *J-V*, (b) *L-V* characteristics and (c) normalized EL spectra of OLEDs with a structure of ITO/ NPB (40 nm)/ TCTA: γ mol. % **1** (20 nm)/ TPBi (30 nm)/ Mg: Ag (150 nm)/ Ag (50 nm), $x = 2, 4, 6, 8$ or 10 .

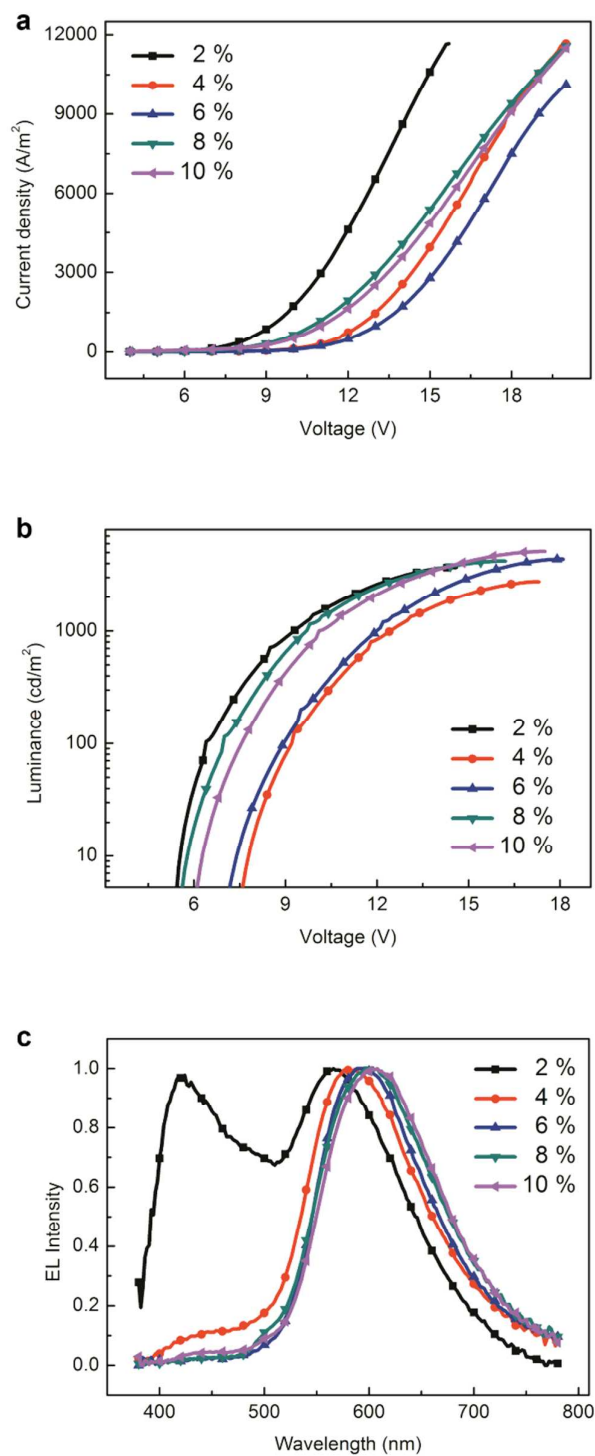


Figure 7. (a) *J-V*, (b) *L-V* characteristics and (c) normalized EL spectra of OLEDs with a structure of ITO/ NPB (40 nm)/ DIC-TRZ: γ mol. % **2** (20 nm)/ TPBi (30 nm)/ Mg: Ag (150 nm)/ Ag (50 nm), $x = 1, 2, 4, 6, 8$ or 10 .

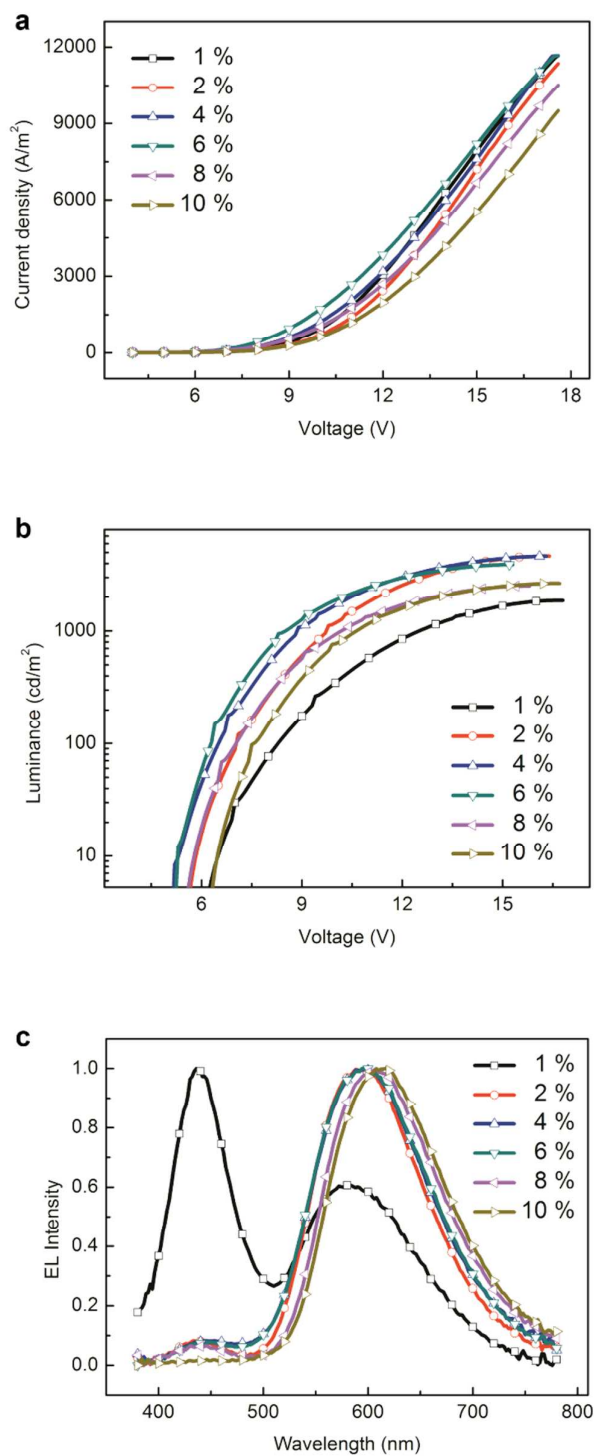


Table 1. Photophysical and electrochemical properties of **1** and **2**.

	Absorption ^a	In solution ^b		In neat film			Redox ^e	
	λ (nm) [ϵ ($\times 10^4$ M ⁻¹ cm ⁻¹)]	λ (nm)	ϕ [τ (μ s)]	λ (nm) ^c	λ (nm) ^d	ϕ [τ (μ s)]	E_{ox} (V)	E_{red} (V)
1	262 [5.73], 372 [1.68]	632	0.01 [0.07]	599	600	0.22 [0.32]	-1.62	0.88
2	266[5.01], 372 [1.02]	631	0.02 [0.05]	597	598	0.21 [0.32]	-1.61	0.89

^a) In acetonitrile solution (1×10^{-5} M), ϵ denotes the molar extinction coefficients. ^b) In degassed acetonitrile solution (1×10^{-5} M), sh denotes the shoulder wavelength, ϕ in solution was measured *versus* [Ru(bpy)₃]Cl₂ ($\phi = 4.0$ % in non-degassed water) as the reference.³⁹ ^c) In neat film prepared by spin-coating in a glove box filled with nitrogen. ^d) In neat film prepared by vacuum evaporation deposition under a low pressure of about 1×10^{-4} Pa. ^e) In degassed N, N-dimethyl formamide (DMF) solution (1×10^{-3} M). Potentials were recorded *versus* the ferrocenium/ ferrocene (Fc⁺/ Fc) couple.

Table 2. Device performance of vacuum-evaporated OLEDs with **1** and **2** doped into the DIC-TRZ host material.

	x^a	V_{on} (V) ^b	Max CE (cd A ⁻¹) [EQE] ^c	Max L (cd m ⁻²) ^d	EL (nm) ^e	CIE ^f
1	4	5.5	3.0 [1.5 %]	13.1×10^3	596	(0.53, 0.46)
	6	5.7	4.5 [2.2 %]	19.4×10^3	596	(0.52, 0.46)
	8	6.6	2.8 [1.4 %]	11.5×10^3	596	(0.52, 0.45)
2	4	5.5	4.5 [2.2 %]	11.3×10^3	596	(0.52, 0.45)
	6	5.6	5.1 [2.5 %]	11.1×10^3	596	(0.52, 0.46)
	8	6.2	3.7 [1.8 %]	12.0×10^3	596	(0.52, 0.46)
	10	7.5	4.5 [2.2 %]	9.8×10^3	596	(0.53, 0.45)

^a) Device structure, ITO/ NPB (40 nm)/ DIC-TRZ: x mol. % Emitter (20 nm)/ TPBi (30 nm)/ Mg: Ag (150 nm)/ Ag (50 nm). ^b) V_{on} , turn-on voltage to reach the luminance of 1 cd m⁻²; ^c) CE, current efficiency; EQE, external quantum efficiency. ^d) L, luminance. ^e) EL, electroluminescence wavelength. ^f) CIE, Commission Internationale de l'Elairage.

Table 3. Device performance of vacuum-evaporated OLEDs with **1** and **2** doped into the TCTA host material.

	y^a	V_{on} (V) ^b	Max CE (cd A^{-1}) [EQE] ^c	Max L (cd m^{-2}) ^d	EL (nm) ^e	CIE^f
1	2	5.4	1.8 [0.9 %]	3.7×10^3	430 (sh), 566	(0.33, 0.34)
	4	7.5	2.1 [1.0 %]	2.8×10^3	578	(0.47, 0.45)
	6	6.9	3.4 [1.8 %]	4.4×10^3	592	(0.52, 0.45)
	8	5.5	2.1 [1.0 %]	4.2×10^3	608	(0.52, 0.45)
	10	5.9	1.8 [0.9 %]	5.1×10^3	608	(0.52, 0.44)
2	1	6.0	0.5 [0.4 %]	1.9×10^3	436, 582 (sh)	(0.32, 0.27)
	2	5.5	2.1 [1.0 %]	4.7×10^3	596	(0.50, 0.44)
	4	5.1	2.8 [1.4 %]	4.6×10^3	596	(0.50, 0.44)
	6	5.2	2.5 [1.2 %]	3.9×10^3	596	(0.49, 0.44)
	8	5.5	1.1 [0.5 %]	2.5×10^3	608	(0.53, 0.42)
10	6.2	1.7 [0.8 %]	2.7×10^3	608	(0.55, 0.43)	

^{a)} Device structure, ITO/ NPB (40 nm)/ TCTA: y mol. % Emitter (20 nm)/ TPBi (30 nm)/ Mg: Ag (150 nm)/ Ag (50 nm). ^{b)} V_{on} , turn-on voltage to reach the luminance of 1 cd m^{-2} ; ^{c)} CE , current efficiency; EQE , external quantum efficiency. ^{d)} L , luminance. ^{e)} EL , electroluminescence wavelength. ^{f)} CIE , Commission Internationale de l'Éclairage.

Table of content

OLEDs are fabricated by vacuum evaporation deposition of novel sublimable cationic iridium complexes, achieving efficient orange-red and white emission.

